Sensor and Simulation Notes

Note 471

February 1999

Radiated Field Measurements from a 1-m Diameter Half IRA

J. Scott Tyo and Jon S.H. Schoenberg
Air Force Research Lab/Directed Energy Directorate

Abstract

A limited set of E-field measurements has been presented preciously for a 1-m diameter half-IRA (HIRA) by Bowen and Farr in SSN 419. In that paper, measurements were reported that were made on boresight at ranges of 1, 3, 10, and 20 meters, and limited azimuth and elevation scans were also performed. However, for a variety of proposed applications for the HIRA, more comprehensive knowledge of the evolution of the near- and intermediate-field pattern of the antenna is needed.

In this paper, a more comprehensive examination of the radiated field near boresight of the HIRA is reported in the region leading from the intermediate into the far-field of the antenna. In addition, data are reported from field mappings throughout the half-space above the ground plane of the HIRA. These data will enable the prediction of field patterns near HIRAs and full reflector IRAs, and should also be useful in characterizing the fields from other similar UWB antennas.

1. Introduction

The half IRA (HIRA) is an unbalanced UWB antenna made up literally of half of a reflector IRA over a truncated ground plane [1]. The nature of the HIRA geometry makes it well suited to mating onto a number of high-power UWB sources, such as the H-series of devices, that have unbalanced, coaxial outputs [2]. A point transition from the coaxial source output to the TEM horn feed structure allows a good wideband transition without the use of a balun. In addition, the partial ground plane provides a natural "hiding spot" for the supporting equipment, e.g. the source, instrumentation, etc.[1]

The prompt radiation on boresight of an IRA is well understood [3], and the prompt radiation from the HIRA is expected to be nearly identical to that from the full antenna. The HIRA studied in this investigation is a 1-m diameter dish over a truncated "triangular" ground plane. The antenna under test is described in detail in [4]. While the boresight radiation is well understood from an IRA, there are only a limited number of theoretical studies that provide information about off-boresight radiation [5]. Most experimental investigations are concerned only with the boresight field, and even when off-boresight radiation is considered, typically only an azimuthal and/or elevation scan is presented [4,6]. In this note, the radiation from the HIRA described in [4] is investigated in detail near boresight, as well as more coarsely in the half-space above the ground plane. In addition, the effect of ground-bounce is explored for the boresight radiation because of the interest for a variety of potential applications of this class of antenna.

2. HIRA Field Mapping – Single Range

The first measurements performed in this investigation involved a comprehensive field mapping of the HIRA at ranges near to the intermediate/far-field transition of the antenna. Comprehensive, simultaneous azimuth and elevation scans were performed in order to characterize the radiation in the half-space above the ground-plane (as well as limited scans performed at negative elevation angles corresponding to locations *beneath* the ground plane). Both free-field and ground-bounce measurements were performed.

2.1. Free-Field Measurements

The free-field data reported below were obtained at two different facilities. The first set of measurements at a range of 17.55 meters were performed in the HEML anechoic chamber, and the second set of measurements at a range of 26.58 meters were performed outdoors near the HERTF facility on the East side of Kirtland AFB.

2.1.1. Experimental Setup

The experimental setup used in the HEML anechoic chamber is depicted schematically in fig. 1. The antenna under test was positioned on a Bogen 3051 tripod with Bogen 3047 tripod head resting on a support at a height of approximately 75 cm above the chamber floor. The tripod head allowed 3-axis control, which was essential for this set of experiments. Because of the ultra-wideband (UWB) characteristic of the radiated waveforms and the high angle of incidence associated with long range measurements, the anechoic material was inadequate to

prevent ground bounce. In order to eliminate this feature from the waveforms, the sensor antenna had to be elevated so that the path-length difference between the direct ray and the specular ray was longer than the desired acquisition time (3 ns). To accomplish this, the sensor antenna was also mounted on a Bogen 3051 tripod with Bogen 3047 tripod head placed on top of the "Trojan Horse", an elevated platform made of wood to be used for just such purposes. Data was taken at slant distances of 17.55 m and 21.64 m as measured by stringing a rope from the source to the receiver. In order to allow for both elevation and azimuth scans to be made, the tripod supporting the source antenna had to be tilted until the vertical axis of the half IRA (HIRA) was parallel to the vertical (azimuth) axis of the tripod/head. This positioning allowed the elevation and azimuth axes to be controlled independently. Because the maximum distance that could be obtained in the HEML chamber was insufficient to reach the far-zone, measurements were also made outside at the HERTF facility at a range of 26.58 m. The measurement location straddled an arroyo immediately south of the blast pad east of HERTF. The range measurement at HERTF was made using a laser-range-finder.

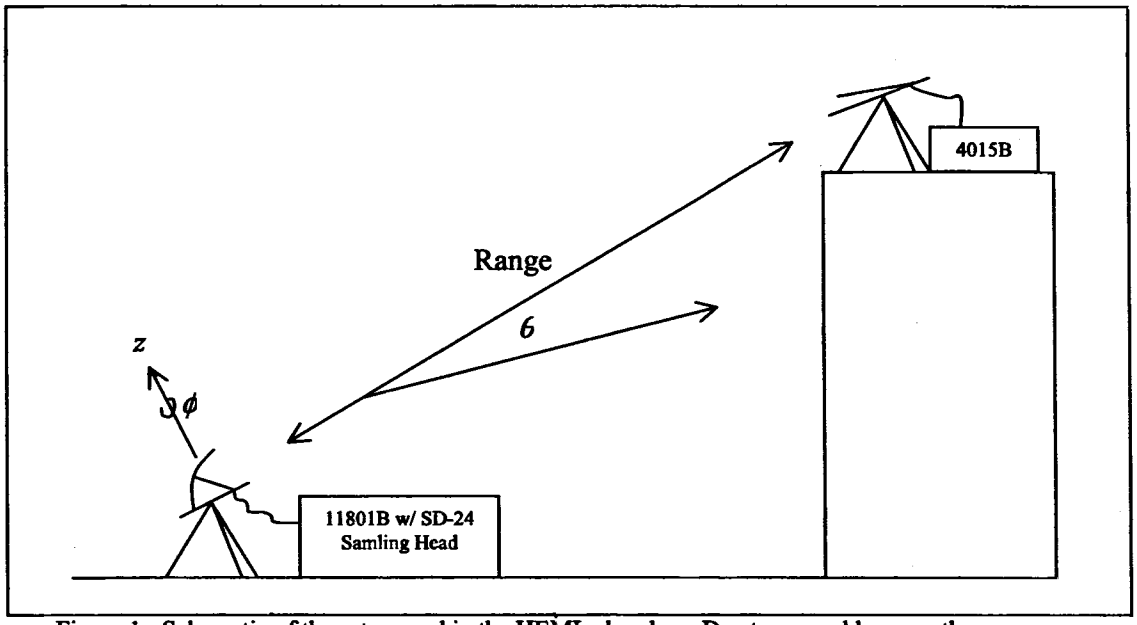

Figure 1: Schematic of the setup used in the HEML chamber. Due to ground bounce, the sensor antenna had to be elevated to increase the path-length difference between the main and reflected rays.

The sensor antenna used for these experiments was a 50-Ω TEM horn prototype sensor manufactured by Farr Research. The sensor is depicted in fig. 2A. The sensor calibration was performed on the AFRL/DEHP UWB antenna range, and the step response of the probe is depicted in fig. 2B.

The source used for this set of experiments was a Picosecond Pulse Labs (PSPL) Model 4015C pulser. The source puts out a –4V, 4-ns duration step with a risetime of 15 ps. The source is connected to its remote sharpening head (PSPL Model 4015 RPH) via a 1′ length of semi-flexible cable provided by the manufacturer. The 4015C is designed to feed a 50-Ω load.

For purposes of convenience, the source was connected to the sensor antenna instead of the antenna under test. All measurements were made using a Tektronix model 11801B Digital Sampling Oscilloscope with an SD-24 TDR sampling head. The sampling head was attached to the HIRA by means of a 2.5-ns length of cable. The measurement system (source, sharpening head, cable, sampling head, and oscilloscope) had a measured risetime of 28 ps. The source was run in external triggering mode, and the trigger signal was generated by the internal clock of the oscilloscope. The trigger output of the oscilloscope was connected to the trigger input of the 4015C through a 115-ns length of RG-214 cable.

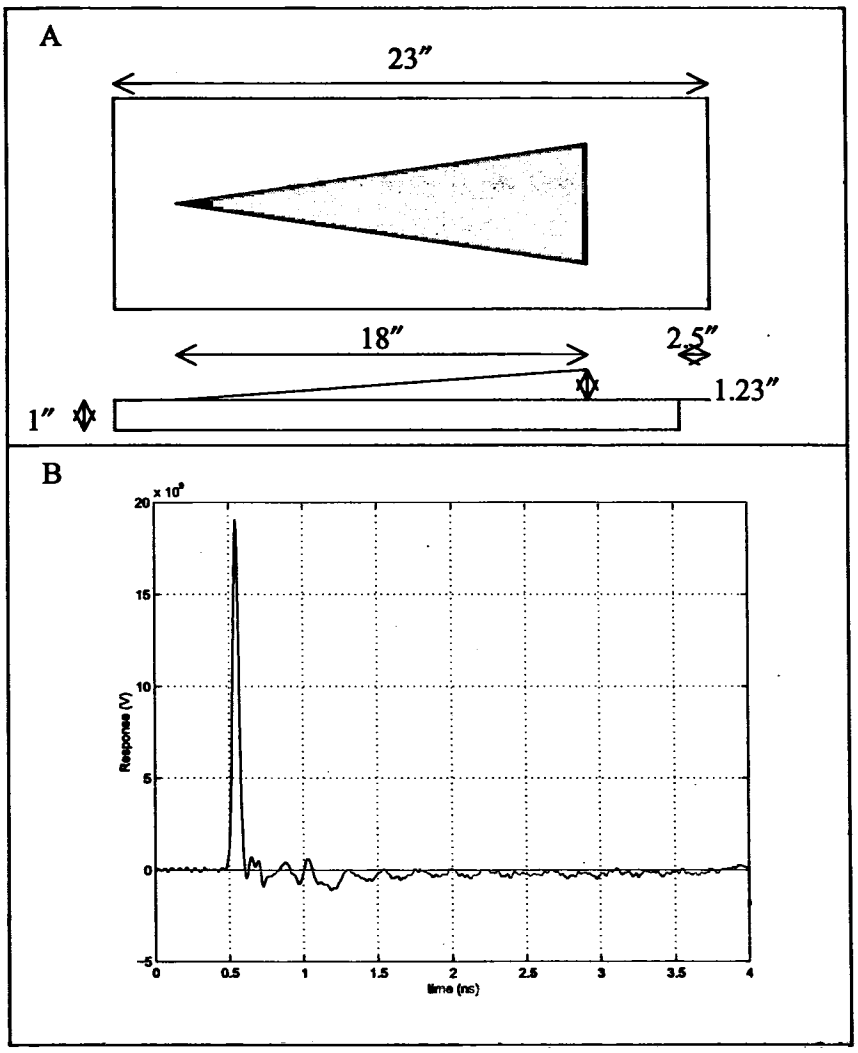

Figure 2: TEM horn sensor used in measurements. A schematic of the sensor is depicted in panel A, and the impulse response (as measured on the AFRL/DEHP antenna range) is shown in panel B. The sensor was manufactured by Farr Research.

2.1.2. Testing Procedures

The purpose of this set of measurements was to develop a thorough picture of the time-domain radiation pattern from the HIRA. Towards this end, measurements were made at several azimuth and elevation angles at two different ranges. In addition to detailed examination of the waveforms radiated in specific directions, the antenna beamwidth in both elevation and azimuth was measured at ranges of 17.55 m (HEML), 21.64 m (HEML), and 26.58 m (HERTF). These beamwidths are listed in Table 1.

Range	Half-Power (az)	Half-Field (az)	Half-Power (el)*	Half-Field (el)*
17.55 m	1.13°	2.05°	4.10°	6.30°
21.33 m	1.25°	2.05°	3.10°	4.90°
26.58 m	1.17°	1.65°	3.60°	4.80°

Table 1: Scale model HIRA beamwidths in azimuth and elevation. *Note, the beamwidth measurements reported are half-width. The elevation measurements are reported above the ground plane only.

Data were collected in the field and stored in the non-volatile memory of the oscilloscope. Data were downloaded from the oscilloscope to a 486-based PC platform using Labview over a GPIB connection. The measured impulse response of the system (Fig. 2B) was then deconvolved from the data using Fourier domain methods. All processing was performed on a Pentium based PC system using Matlab (ver. 5.1).

2.1.3. Results and Discussion

Measured field waveforms are presented in figs. 3-9 in various forms. Fig. 3 compares the measured field at the two different distances with two different time bases. The expected features of the radiated waveforms are all clearly identifiable. The negative prepulse due to direct radiation from the feed [7] can be identified in fig. 3A. It is of low amplitude and a duration equal to the time necessary for the main beam to travel up the TEM feed to the parabolic reflector and back to the plane that includes the feed and is normal to the axis of the reflector (0.76 m or 2.55 ns for the HIRA). The prompt portion of the waveform follows. This is opposite in polarity with respect to the prepulse due to the reflection from the metal surface of the reflector. The width of the pulse is related to the risetime of the step generator (see discussion in Sec. 4.4. below). The peak radiated field is related to the dV/dt of the step generator, the effective height of the antenna, and feed impedance of the HIRA, and the range as discussed in [17]. What occurs after the impulse is more difficult to quantify analytically, but in actuality has little influence on the spectral content of the waveform.

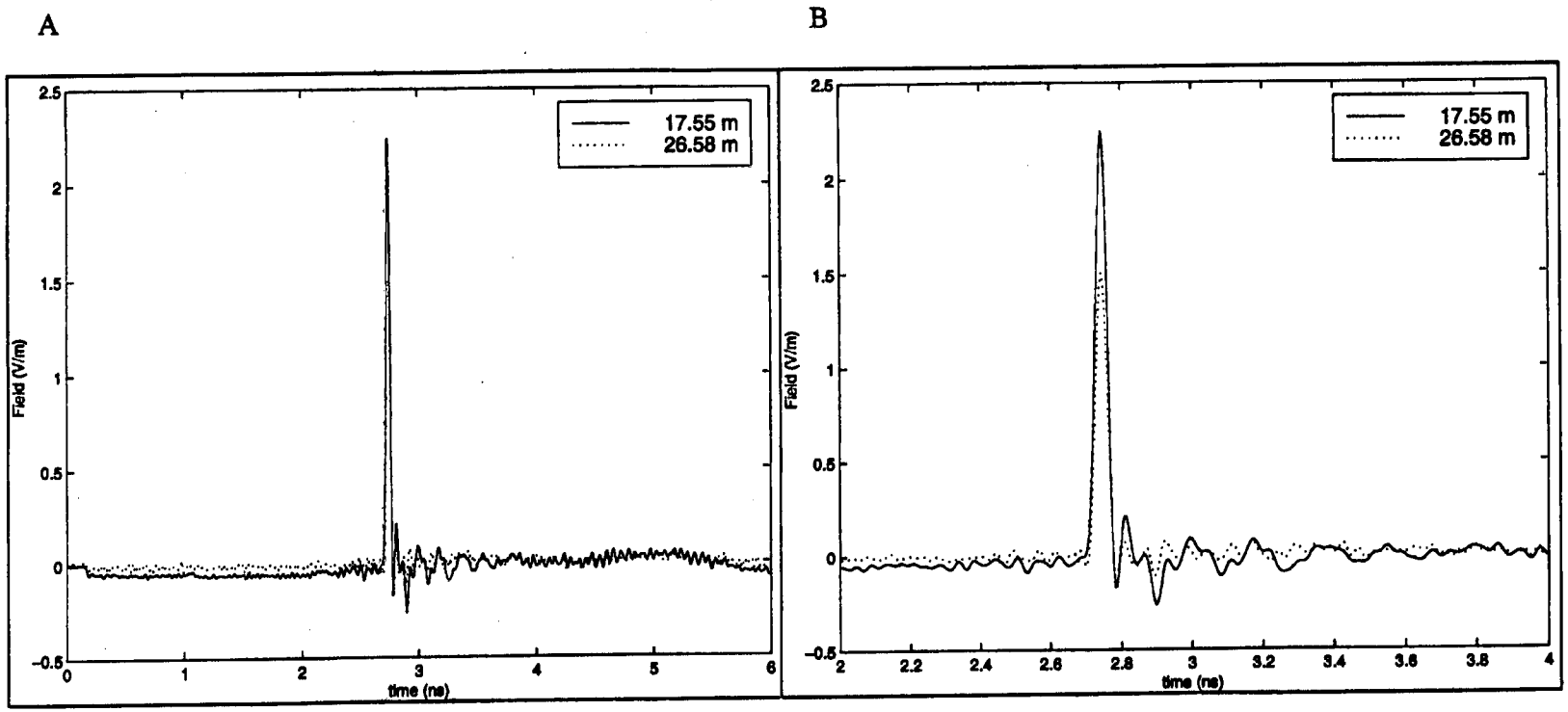

Figure 3: Radiated field on boresight at ranges of 17.55 m and 26.58 m. The prepulse is clearly discernable in panel A. The close up view of the main pulse in panel B shown the expected differentiating behavior of the HIRA on boresight as the far-field is approached.

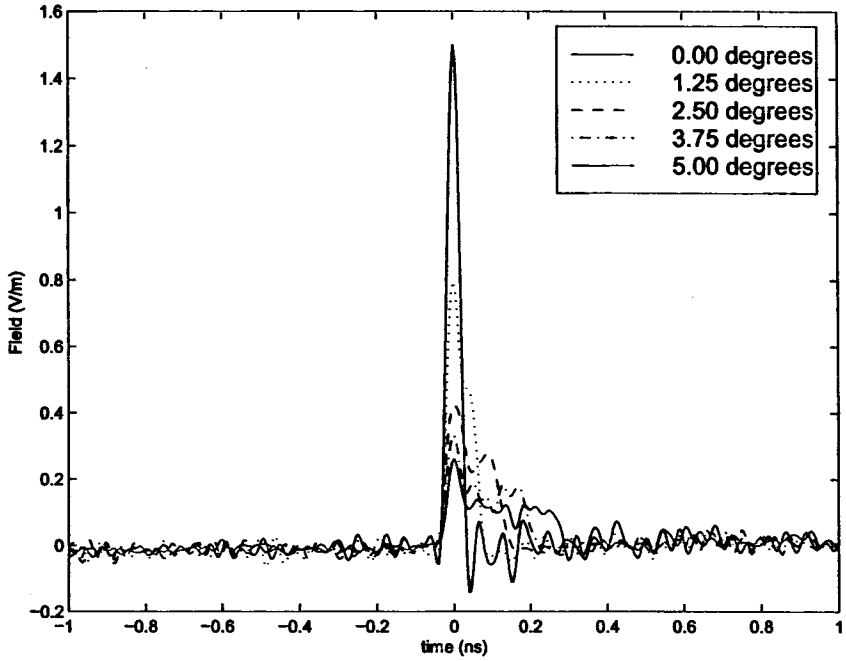

Figure 4: Azimuth scan of the HIRA. As the sensor moves off-boresight, the ideal timing breaks down. First, the direction of observation moves away from the direction of focus of the reflector resulting in pulse-broadening. Second, the two feed arms begin to appear at different times, further degrading the field with respect to the boresight waveform.

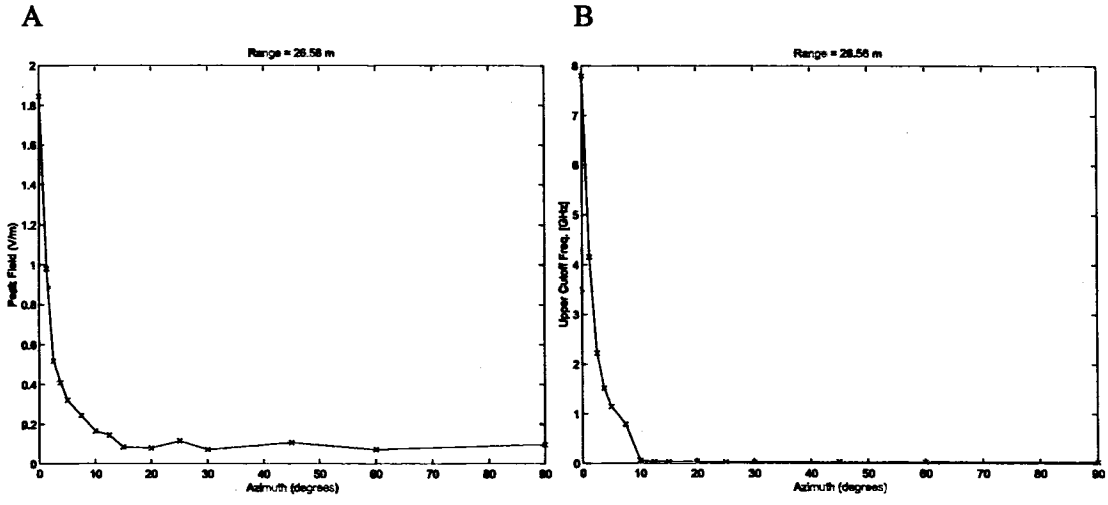

Figure 5: Degradation of the waveform from the HIRA in off-boresight directions. As expected, the peak field drops drastically and the pulse width gets larger very rapidly as the sensor is moved away from the boresight direction.

As the sensor is moved off boresight in azimuth, two distinct processes occur that degrade the waveform. First, the aperture is no longer focused in the direction of view, and the pulse width broadens considerably [5]. Second, the vertical symmetry of the HIRA breaks down as one of the feed arms is closer to the observer than the other. At angles greater than about a degree (in the far-field), the radiation due to each of the two feed arms can begin to be clearly identified, and the pulse width and peak amplitude suffer. These two processes are demonstrated in the data presented in figs. 4 and 5. When the sensor is moved off boresight in elevation, only defocus occurs as the vertical symmetry of the antenna is preserved. Furthermore, the vertical height of the antenna is ½ the horizontal width. Hence, twice the transverse angle is needed in the vertical direction to get similar dispersion [8,9]. Consequently, the degradation of the waveform is not as severe, and the beamwidth is larger in elevation (E-plane) than azimuth (H-plane). The degradation of the waveform in elevation is presented in figs. 6 and 7. Note that in both azimuth and elevation scans the prepulse is still clearly discernable and largely unaltered as expected. Some additional measurements at various angles are presented in fig. 8. A final point of interest is the frequency content of the radiated waveforms. The Fourier transforms of several of the radiated signals are presented in fig. 9.

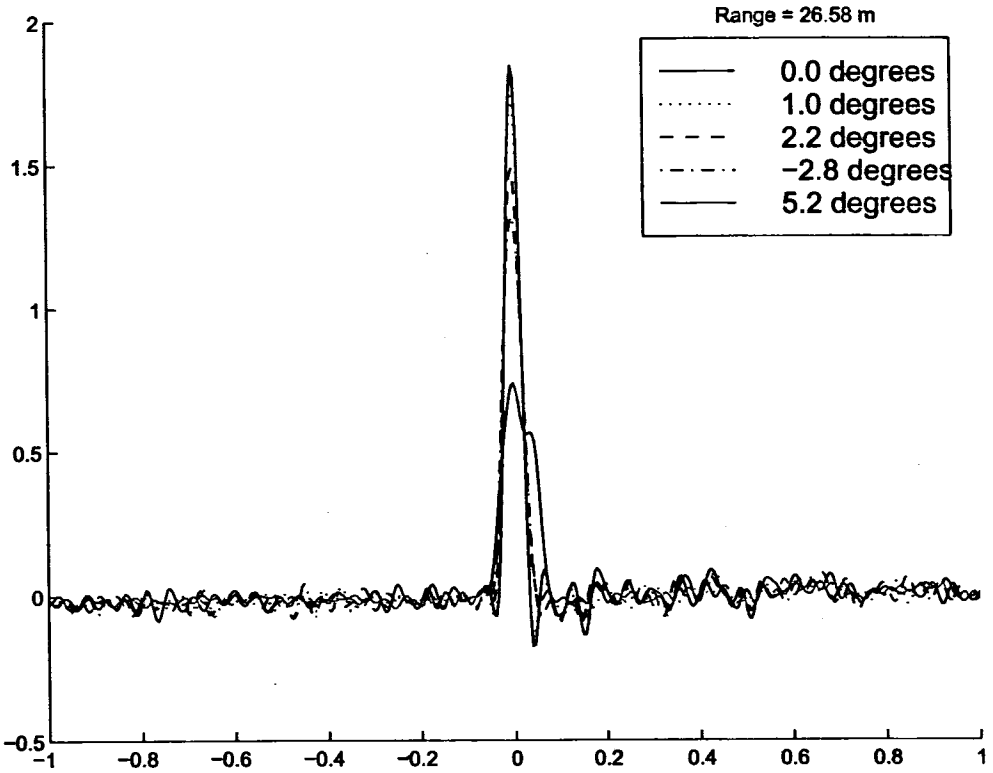

Figure 6: Elevation scan. Most of these measurements were taken *above* the ground plane, but note that there is one measurement taken below the ground plane. The below the ground plane data is especially relevant for the ground-bounce measurements discussed below.

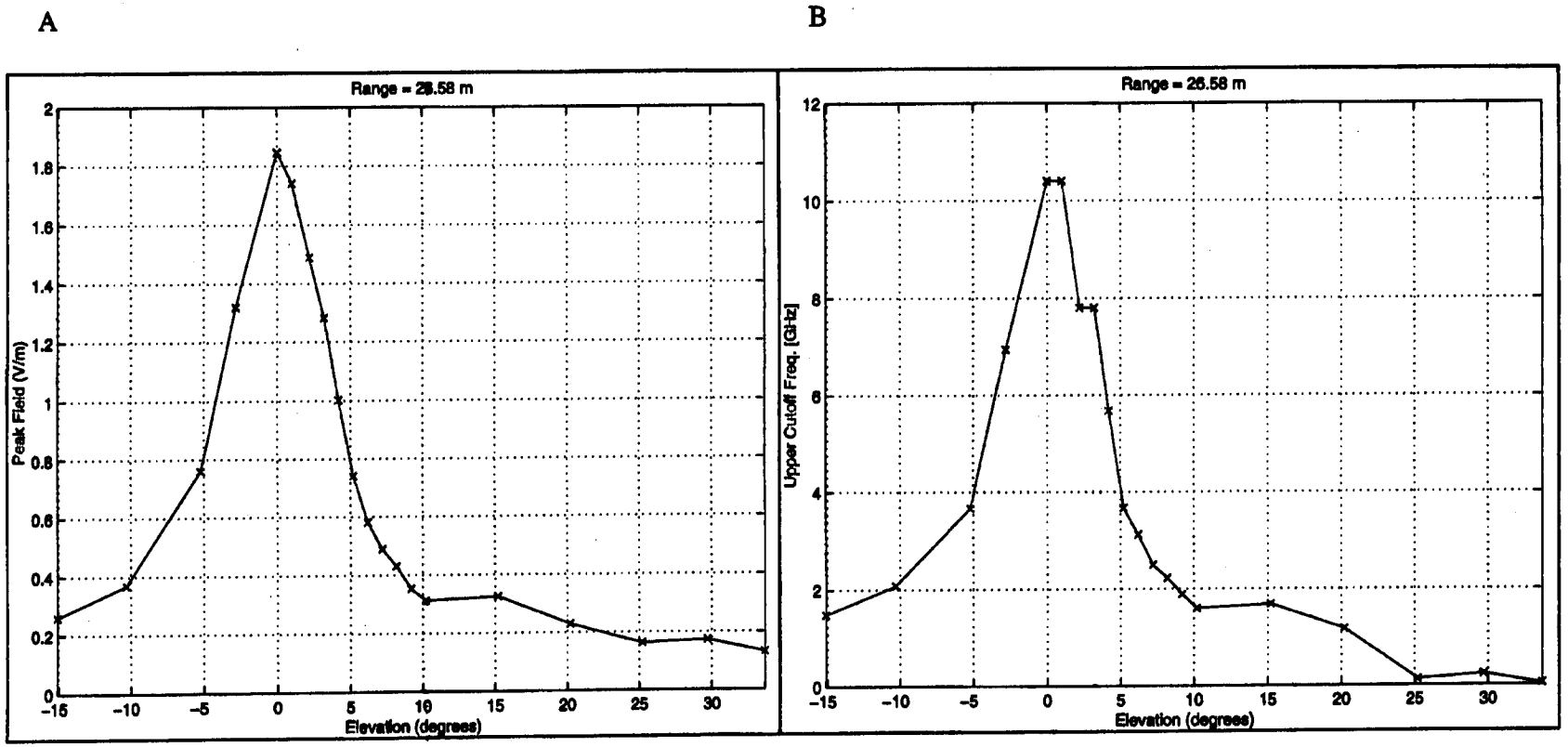

Figure 7: Degradation of the waveform as the sensor is moved off-boresight in elevation.

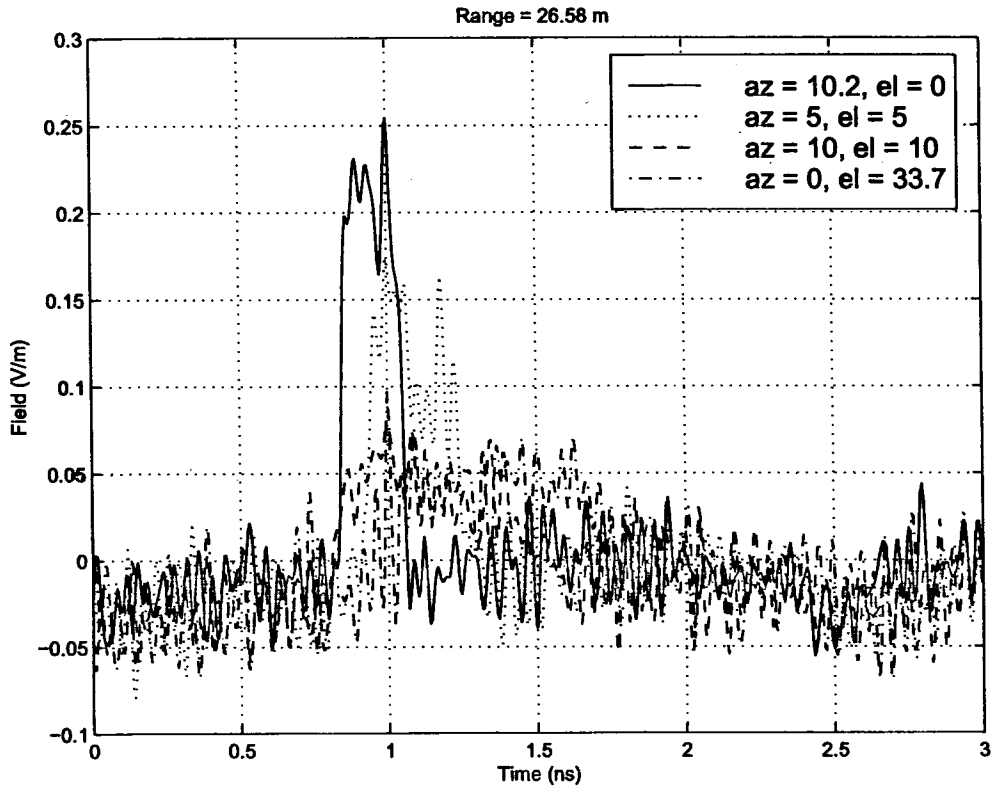

Figure 8: Waveforms taken at various off-boresight locations.

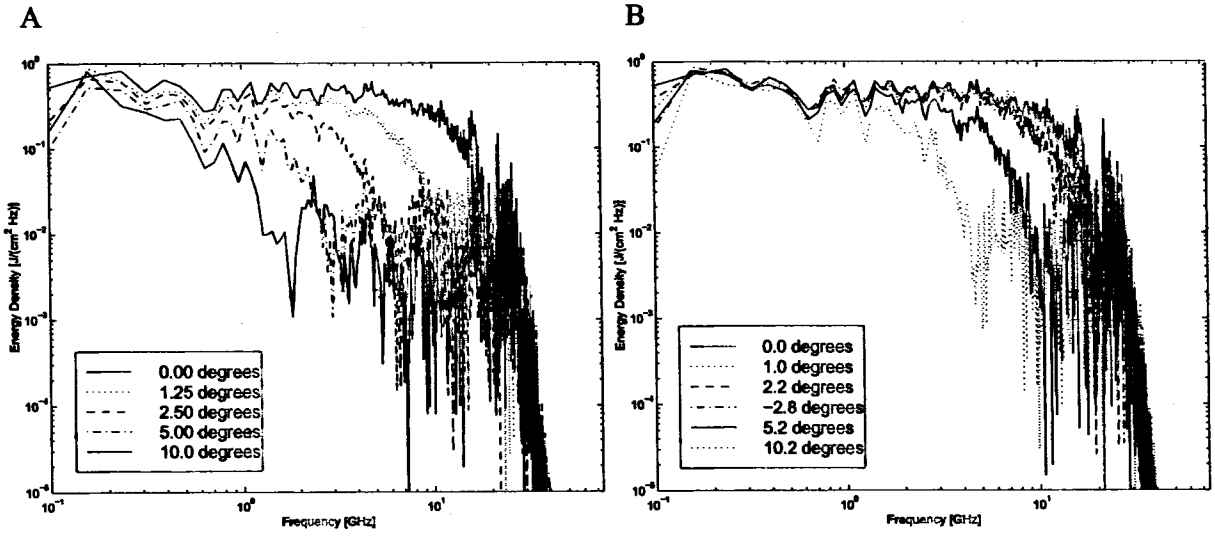

Figure 9: Spectra of the radiated waveforms corresponding to the traces presented in figs. 4 and 6.

2.2. *Ground-Bounce Measurements*

To compare the free-field radiated waveforms to the signals radiated over a flat earth, a ground-bounce measurement was made on the roof of the HERTF facility. The roof is made of reinforced concrete, and the antenna was positioned 3′ above the flat surface. The range was set at 26.82 m. With the exception of the flat earth, all other aspects of the experimental setup remained the same as in the free-field measurements. With the experiment configured as described, the only way to measure the response of the antenna in elevation is to physically raise the sensor (simply tilting the HIRA alters the relationship between the antenna and its environment – the flat earth). This was not feasible, so only the azimuth was varied.

The ground bounce signal is due to reflection of the off-boresight field at the specular point. Because the path length is longer, the ground-bounce signal arrives later in time. The time delay is well approximated by the expression

$$\Delta t \approx \frac{2h_1 h_2}{Dc}, \tag{1}$$

where h_1 and h_2 are the heights of the two antennas above the ground, D is the separation between the antennas, and c is the speed of light. Eq. (1) is valid when $h_1, h_2 << D$. Because the angle of incidence at the specular point is so near to grazing (~4° in the current configuration), the reflection coefficient is significant. However, this specular point is also outside the focused beam of the antenna, and is therefore lower in amplitude. The ground-bounce measurements are summarized in figs. 10 and 11.

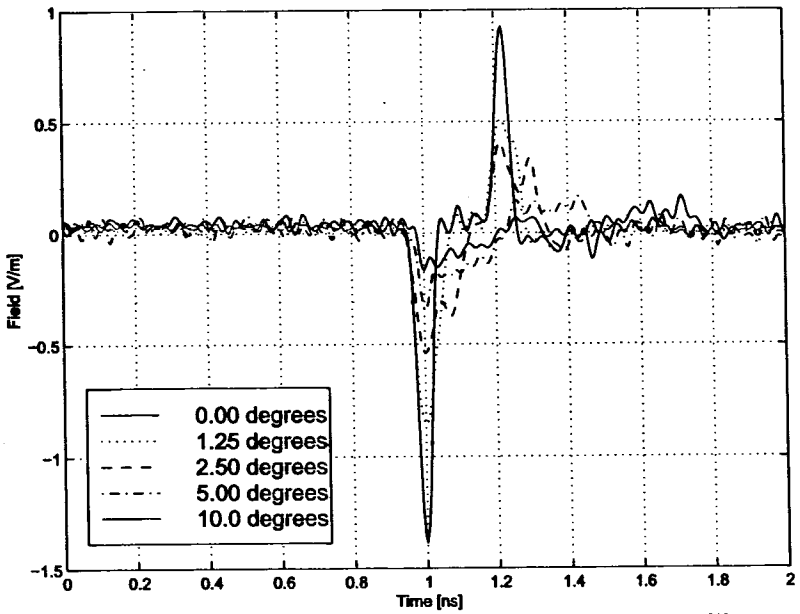

Figure 10: Ground-bounce measurements made at a distance of 26.58 m. The ground bounce arrives later in time and is flipped in polarity relative to the main beam as discussed in the text.

One result should be highlighted here. Fig. 11 shows a clear ripple in the spectrum that is due to the arrival of the ground-bounce signal. The ripple in the frequency domain corresponds to the temporal separation of the ground bounce and the main pulse. Comparing this data with the free-field measurements and later ground bounce measurements (Sec. 4) indicates that the antenna may not have been boresighted properly. First, the pulse width of the main beam in the ground-bounce measurement was 15% larger than the pulse width of the main beam in the corresponding free-field measurement – 40 ps compared with 35 ps. Second, the pulse width of the ground bounce is the same as that of the main beam, whereas in later measurements, the pulse width of the ground bounce is significantly larger than the main beam. Both of these discrepancies might be explained if the HIRA was pointed slightly towards the ground. This would result in a slight widening of the main beam and lowering of the peak amplitude. Comparison of the waveform in fig. 10 with the data in figs. 6 and 7 indicates that the HIRA may have been pointed as much as 2.5° below boresight. This tilt would also have the effect of narrowing the ground bounce signature because the specular point would be further into the boresight of the HIRA. As discussed in Sec. 4, when the ground bounce has a significantly wider pulse width, its effect on the spectrum is less drastic. In either case, if flatness of spectrum is an issue in future designs, the ground bounce signal must be considered.

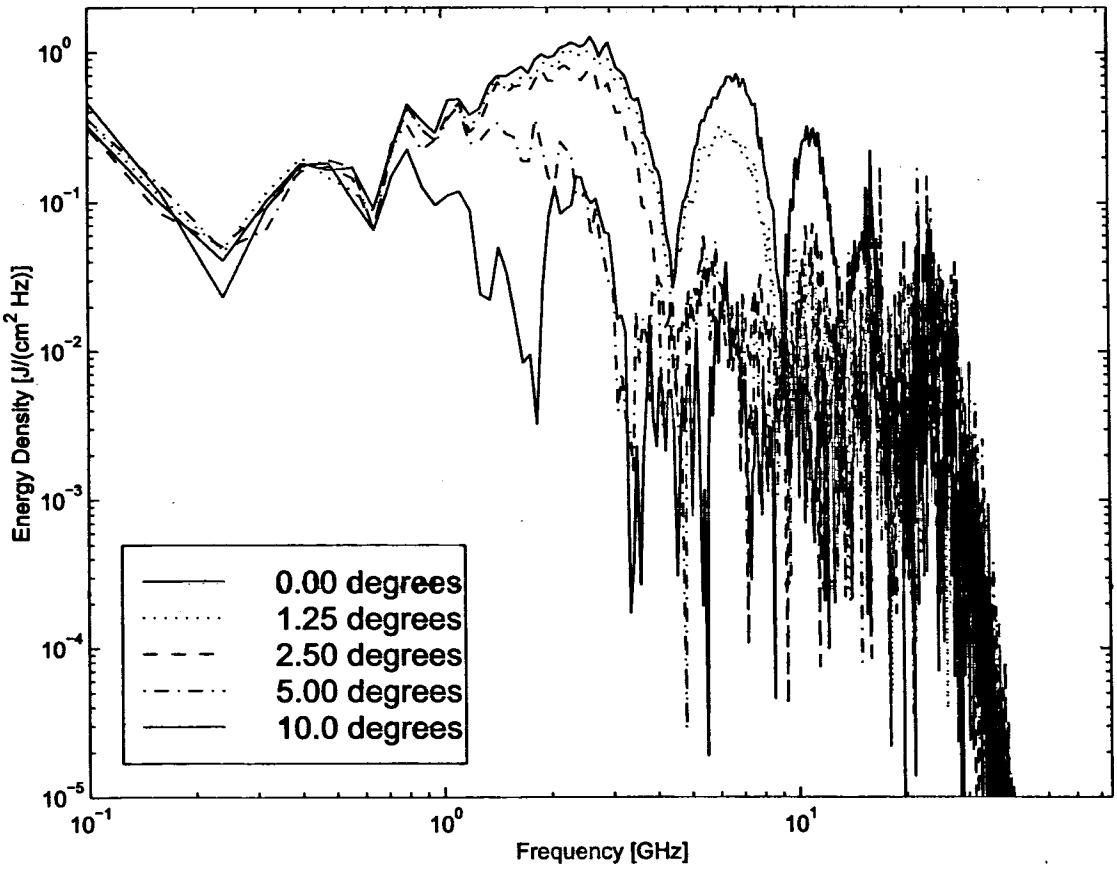

Figure 11: Spectra of the ground-bounce measurements presented in fig. 10.

3. Extreme Near-Field Measurements

In order to characterize the relationship between the peak radiated field and the peak field close to the antenna, a series of measurements was made to the side of the HIRA as well as directly behind the reflector. These measurements were made on the roof of HERTF in the ground-bounce configuration with the TEM-horn sensor depicted in fig. 2. Because the sensor is not electrically small, it is difficult to claim with certainty that the received waveform is *exactly* that which was radiated. The difficulty lies in the fact that the available theory predicts the receive response of a TEM horn when excited by a uniform plane wave [10,11]. Very close to the antenna, the phase front of the wave cannot be approximated as planar, and the field cannot be approximated as uniform over the aperture of the TEM horn sensor. While the exact effects of these perturbations are not known, it should be possible to infer qualitative information about the extreme near fields, especially in the early time.

The setup used for these experiments was the same as that used for the ground-bounce measurements described above, except the long length of trigger cable was replaced by a 15-ns length of RG-58 coaxial cable. The sensor was placed at various locations along the axis of the reflector directly behind the HIRA as well as on the axis that lies at the intersection of the extended ground plane and the plane of the reflector aperture.

The fields and spectra measured along the back and side axes are depicted in fig. 12 and 13 respectively. In both figs. 12 and 13 the back-radiated waveforms are in panel A, the side-radiated waveforms are in panel B. Note that the peak field in the vicinity of the antenna is very close in amplitude to the peak radiated amplitude at a range of ~25 m. While the peak near field happens to be close to that of the radiated boresight field, the waveforms have dramatically different shapes. The radiation in the backward direction is dominated by low-frequency components as should be expected because the high-frequency portions of the waveform are blocked by the reflector. Only the low-frequency components (those which, incidentally, are not radiated well in the far-field on boresight) are able to diffract around the edge of the reflector into the shadow region behind. In contrast, the high-frequency components of the radiation are preserved in the side direction. This is because the radiation is not blocked at all in the side direction due to the configuration of the feed arms. In the near field, the feed arms act like a replicating antenna, and the early-time near field is simply a replica of the drive waveform, i.e. a fast-rising (wideband) step. If large-amplitude, high-frequency energy content is undesirable close to the antenna, then the side radiation must be suppressed [12].

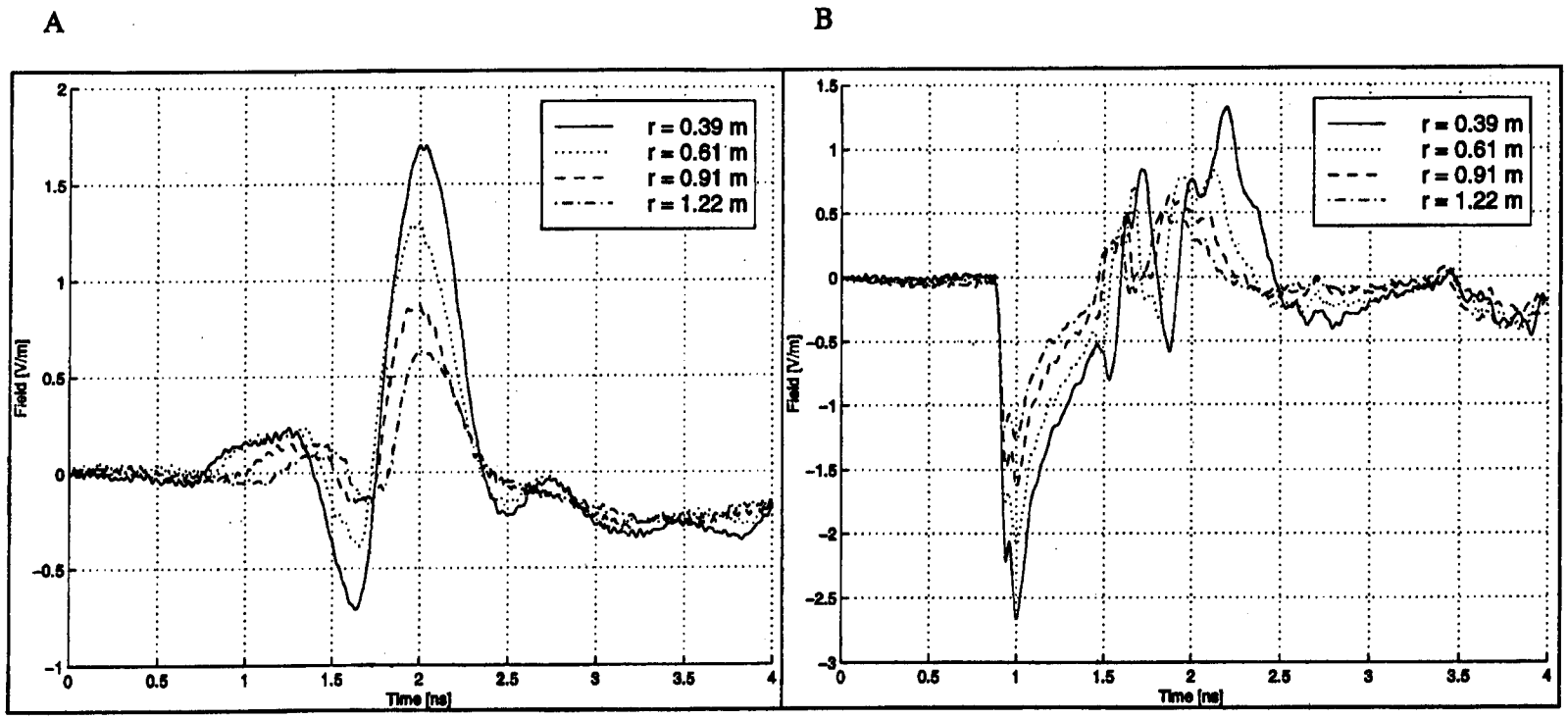

Figure 12: Near-field radiated waveforms in the back (panel A) and side (panel B) directions at the indicated ranges.

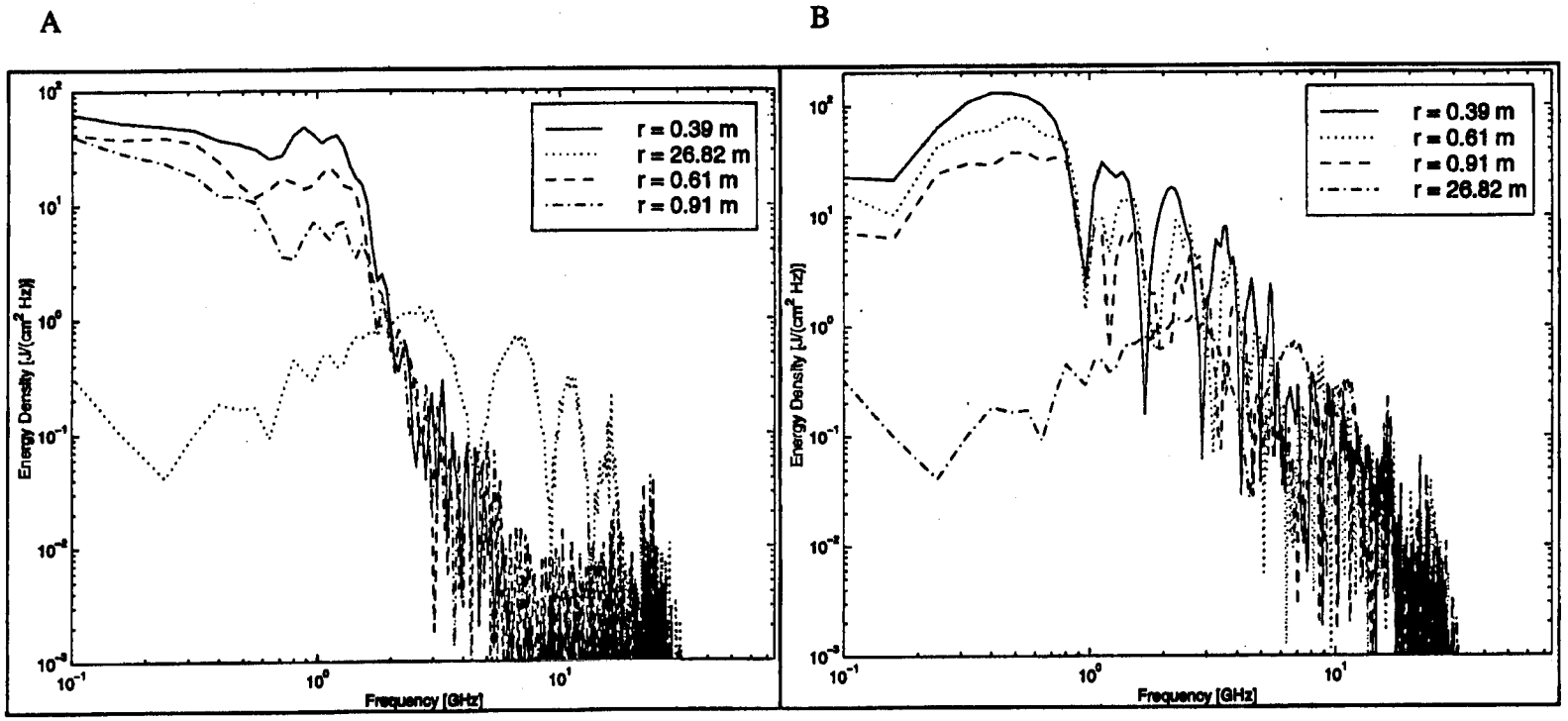

Figure 13: Spectra of the near-field measurements presented in fig. 13.

4. Beam Mapping Measurements

The final set of tests performed in support of this project was a detailed investigation of the extent of the "main beam" of the HIRA. The region of interest for these studies was from seven to 30 meters, the smaller of which is well inside the intermediate-field of the antenna (with 30-ps excitation) and the latter of which is close to the intermediate field-far field transition. While predictions exist for the radiation pattern from a reflector IRA in the far-field [5], the problem of the "intermediate field" of an IRA has not been treated very often [10,13]. For this reason, the intermediate field of the antenna was thoroughly probed in this study. Because of the lack of a single definite means for defining the antenna parameters of a time-domain antenna [14], it is important to define the term "main beam". In this study, we were interested in mapping out the peak field radiated from the antenna as well as the pulse-width (or equivalently the upper cutoff frequency) of the radiated energy.

4.1. Experimental Setup

These measurements were performed using a setup similar to the one used for the ground-bounce measurements reported in section 2.2. The measurements were made in three sessions, two in the HEML anechoic chamber and one on the roof of the HERTF facility. The same setup was used in both sets of experiments, the only significant difference being the nature of the ground. In the HEML anechoic chamber, the floor was metal while the "ground" on the roof of HERTF was reinforced concrete. This difference manifested itself in the sign of the ground-bounce signal. In the former case, the ground-bounce signal has the same polarity as the main pulse, in the latter case, the ground-bounce is inverted with respect to the main pulse. The inversion in the measurements made at HERTF is due to the fact that the angle of incidence is past the Brewster angle, giving a 180° phase shift relative to the reflected wave for normal incidence.

The physical setup of the equipment is essentially the same as that depicted in fig. 1, only modified to be a ground-bounce (rather than free-field) measurement. The HIRA was mounted on a Bogen 3058 tripod with Bogen 3047 3-axis tripod head. The antenna was positioned at a height of 3′ above the ground surface and was leveled using the levels on the tripod. The source used for these experiments was a PSPL 4015B pulser similar to the 4015C described in section 2.1. This particular device outputs a negative step with a specified risetime of 15 ps and a 9.3 V amplitude. The 4015 RPH sharpening head was attached to the HIRA through a 2.5 ns length of 0.141″-diameter semi-rigid cable. The measured system risetime (pulser, sharpening head, cable, sampling head oscilloscope) was 27 ps.

The sensor used for this set of measurements was a balanced, dual 50-Ω output TEM sensor with transmission line extensions to improve the time-domain response. The outputs of the antenna were fed into the two channels of an SD-26 sampling head via 6″ lengths of 0.141″-diameter semi-rigid coaxial cable and digitized by a Tektronix CSA-803 sampling oscilloscope. The sampling head was shielded from the sensor to avoid reflections by a 6″ aluminum wedge that couples to a 6′x4″x2″ hollow rectangular aluminum tube. The sampling head rested inside the wedge/tube and was connected to the oscilloscope using two 2-m extender cables. The sensor was mounted to a Bogen 3058 tripod with Bogen 3047 3-axis tripod head. The antennas

were positioned and rotated manually. The sensor tripod was located at a fixed position and pointed in a fixed direction. A 100′ measuring tape was laid along the ground from the sensor to the HIRA. The source antenna was positioned along this line and rotated using the tripod head.

4.2. Testing Procedures

The purpose of this set of experiments was to characterize the shape of the main beam of the HIRA in a ground-bounce configuration. To accomplish this, the antennas were separated in 3′ increments from 24′ to 99′ and measurements of the prompt radiated signal (main pulse and ground-bounce) were made at several angles. The actual angles used at each distance varied, but the aim was to make measurements up to 1.5 radii (1.5 meters) off the ceterline axis of the HIRA.

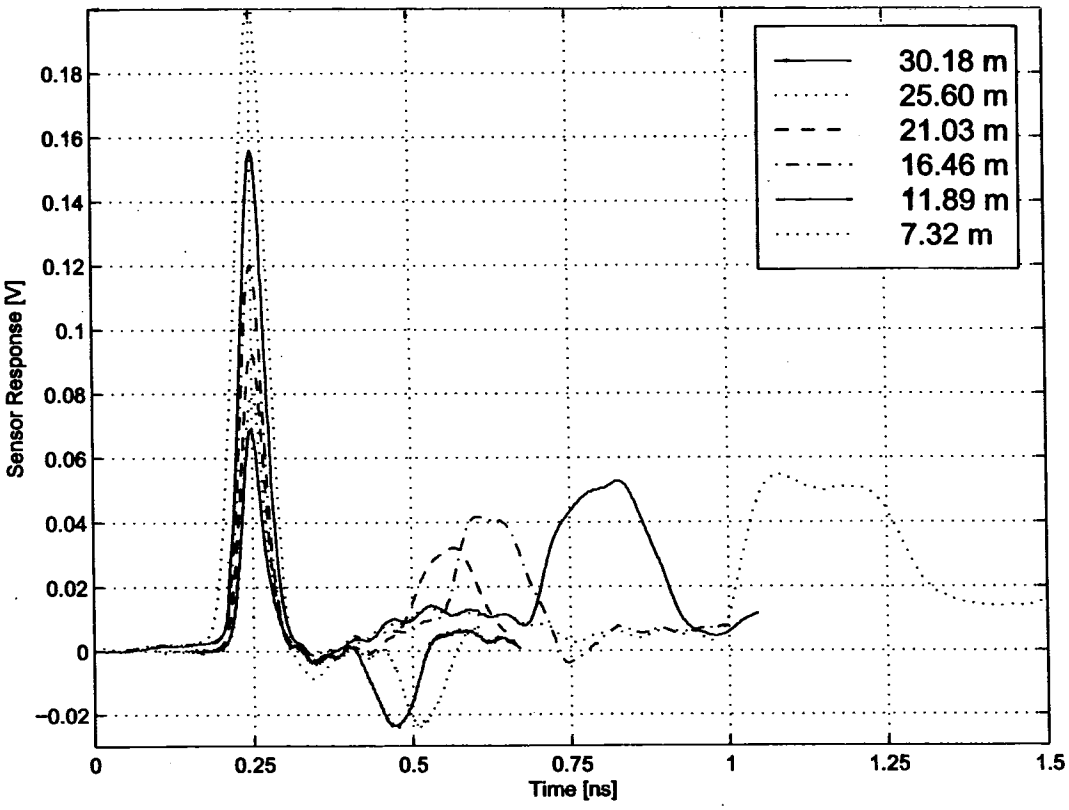

Figure 14: Ground-bounce measurements made in the second set of scale model tests. Note that the polarity of the ground-bounce is different in the farther two traces. This is due to the nature of the ground as discussed in the text. Also, note that as the two antennas get closer, the ground bounce widens because the specular point moves further out of the main beam.

Once the two antennas were positioned, the pulser was triggered in rep-rate mode by the oscilloscope. The two outputs were digitally subtracted in software using the CSA-803, and the resulting waveform was stored in the non-volatile memory of the oscilloscope and later downloaded to a 486-based PC platform using Labview and a GPIB connection. After

downloading, the data was transferred to a Pentium-based PC platform, and the waveforms were analyzed using Matlab (ver. 5.1).

4.3. Results

Examples of processed data and their spectra are presented in figs. 14 and 15. These traces clearly show the main pulse from the HIRA as well as the ground-bounce signal that arrives at a later time given in (1). The main pulse is larger in amplitude and has a significantly shorter pulsewidth. As discussed above, the polarity of the ground-bounce signal is reversed in the long-range measurements made at HERTF (concrete roof) with respect to the measurements made at HEML (metal floor). The characteristic features of the radiated field from a reflector IRA including the variable location of the ground-bounce signal as range changes are present in the measurements shown in fig. 14. The zero point was determined by analyzing the baseline before the main pulse (end of pre-pulse) and the pulsewidth measured was full width half max (FWHM).

In Sec. 2.2. ground bounce data was presented that contrasts slightly with what is seen in figs. 14 and 15. Here, the pulse width of the main beam is significantly shorter than that of the ground bounce signal, meaning that there is little high-frequency content in the second pulse. In fig. 16, we see a comparison of the Fourier transform of *just* the main pulse with the Fourier transform of the entire signal (main + ground bounce) obtained on boresight at 30.18 m. Once again there is ripple introduced in the spectrum due to the arrival of the ground bounce signal. The nulls are not as deep in fig. 15 as they are in fig. 11, and the effect at high frequencies is less pronounced. However, it is important to reiterate that if flatness of the spectrum is an issue in the presence of a ground-bounce signal, measures must be taken to suppress it.

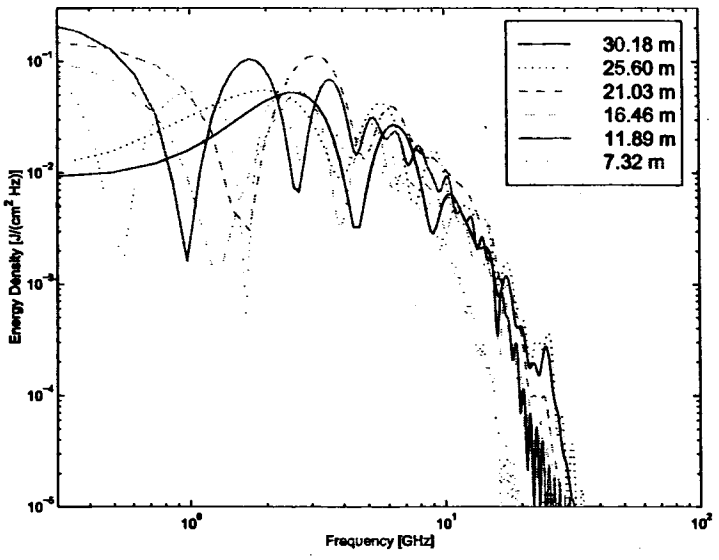

Figure 15: Spectra of the plots presented in fig. 14.

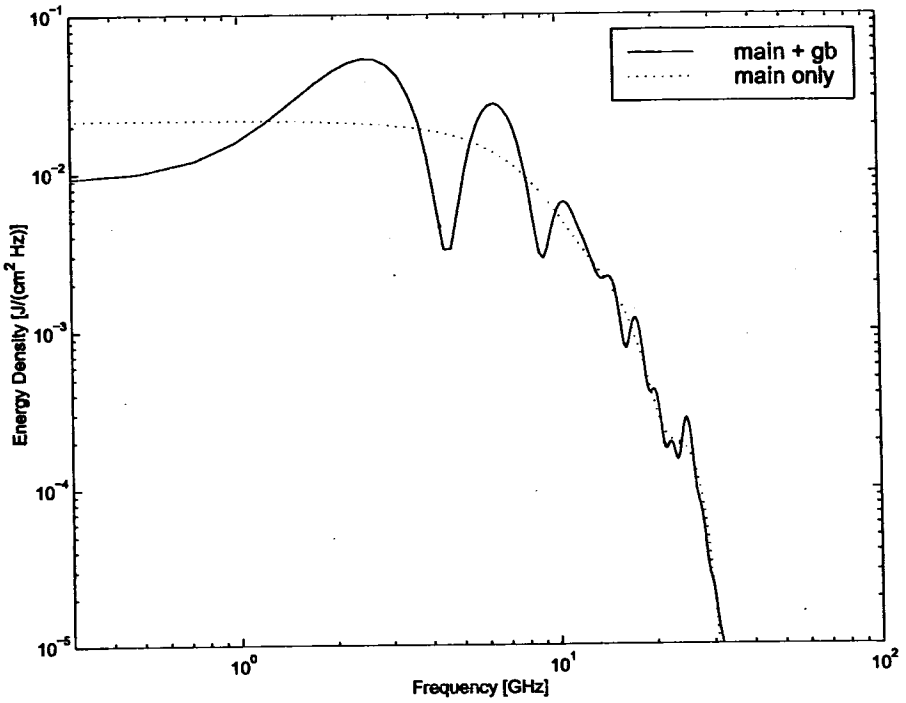

Figure 16: Spectra of the main pulse only (padded with zeros) and the whole trace (including ground bounce). This plot clearly shows the rippling effect that is due to the late arrival of the ground-bounce signal.

The primary parameters of interest were peak field and upper cutoff frequency. These parameters are mapped out in the plane of the ground plane in figs. 17-19. Fig. 17 depicts the distribution of both the peak field and the 3 dB cutoff frequency in the main beam, fig. 18 depicts a contour plot of the peak field data, and fig. 19 presents a contour plot of the cutoff frequency data. It should be noted that the 3 dB cutoff frequency was calculated from the pulsewidth, not from actual measurements of the Fourier transform, and was determined from the *main pulse only*. This procedure was used because the sampling resolution in the frequency domain was only on the order of 1-2 GHz (depending on the exact window size used) and the ground bounce signal depends on the exact experimental configuration, while the main pulse does not depend on the setup. The formula used to estimate the 3 dB pulsewidth was that for a Gaussian pulse:

$$f_{3\mathrm{dB}} = \frac{0.3120}{t_{FWHM}}. \tag{2}$$

Comparison of the predictions of (2) with the actual Fourier transformed data (main pulse only) showed good agreement, especially within 1° of boresight when the radiation from the two feed arms is indistinguishable.

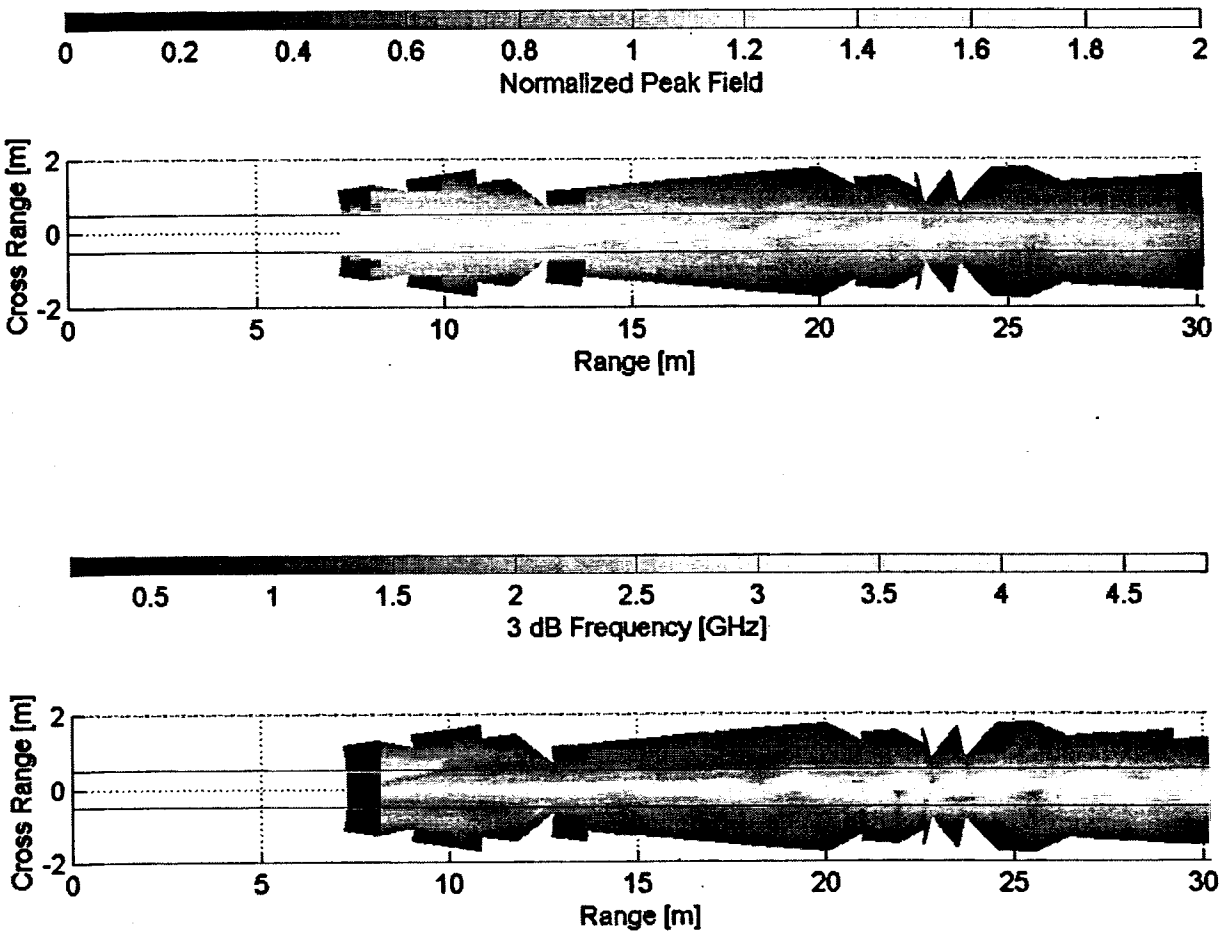

Figure 17: Beam pattern in the intermediate field of the HIRA. Top plot shows the evolution of the peak field, bottom plot shows the evolution of the pulse width.

4.4. Conclusions

From the data presented in figs. 14-19, certain conclusions can be drawn about the shape of the main beam of the HIRA in the intermediate field. Regarding the peak field, the beam seems to emanate from the physical dimensions of the reflector, expand somewhat in the near field, perhaps to a width of 2-2.5 reflector diameters, then contract once again as the far-field is approached. This behavior is expected, and agrees well with established theory regarding the radiation from an IRA near boresight where the peak field on boresight is expected to fall off as $1/r$ as the far-field is approached [4,5,15,16,17].

In analyzing the pulse width measurements, the data presented in figs. 17 and 19 is seen to agree well with the boresight predictions for the behavior of the radiated waveform as the range increases. In [17], the approximate delta function $\delta_a(r,t)$ was introduced. This function is a constant area square pulse with a width that decreases as $1/r$ (and correspondingly an

amplitude that increases as r). The far-field is reached when $\delta_a(r,t) \rightarrow \delta(t)$ and the pulse width of the radiated field is approximately given by the risetime of the input step[1]. In the intermediate field, the derivative of the input step must be convolved with $\delta_a(r,t)$, and the corresponding pulse width is increased. We see in figs. 17 and 19 that the pulse width does indeed decrease as the range approaches the far field. It would be expected that the pulse width should asymptote to a constant value once the far-field is reached, but additional measurements would be necessary to verify this. In [10], it is determined analytically that in the extreme near field the peak field is constant, but additional measurements are necessary to validate this as well.

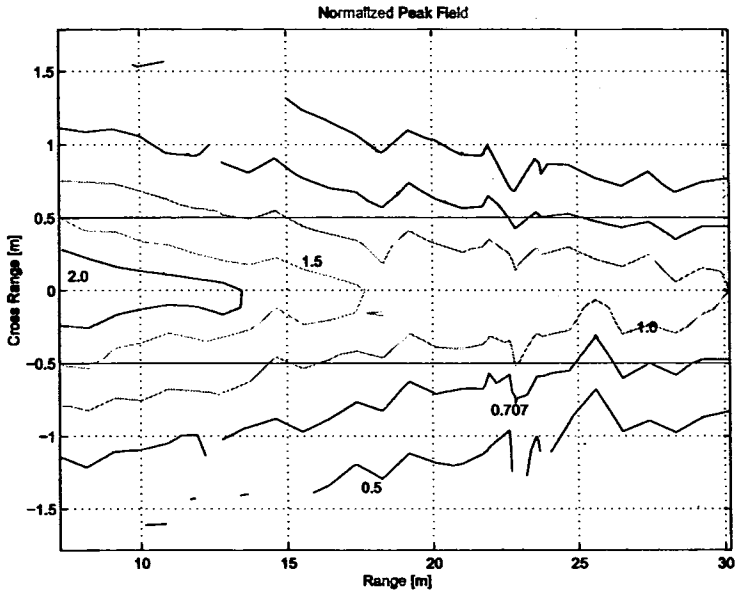

Figure 18: Contour plot showing contours of constant peak field in the intermediate-field of the HIRA. The beam initially widens, then narrows as the far-field is approached.

One final point that is interesting to explore at this time is whether the far-field of the antenna had been reached for the risetime of the excitation used in this experiment. There are many possible definitions for the far-field of a time domain antenna, but three potential empirical definitions are: 1) the range after which the amplitude on boresight decreases as $1/r$; 2) the range after which the radiation pattern is a function of angle only; or 3) the range after which the pulsewidth of the radiated boresight field is constant.

The first of these definitions is considered in fig. 20. In fig. 20, the measured peak field on boresight is compared to a curve that decays as $1/r$ and is fixed to pass through the value at the longest range (30.18 m). As can be seen from the data, beyond ~22 m, the peak radiated field on boresight does indeed fall off as 1/r, indicating that the longer ranges may be on the far-field side of the intermediate- /far-field transition zone. At ranges shorter than 22 m, the field

[1] If the input waveform to a differentiator is an error function step with 10%-90% risetime t_{10-90}, the differentiated field is a Gaussian with FWHM pulsewidth of $t_{FWHM} = 0.919 t_{10-90}$.

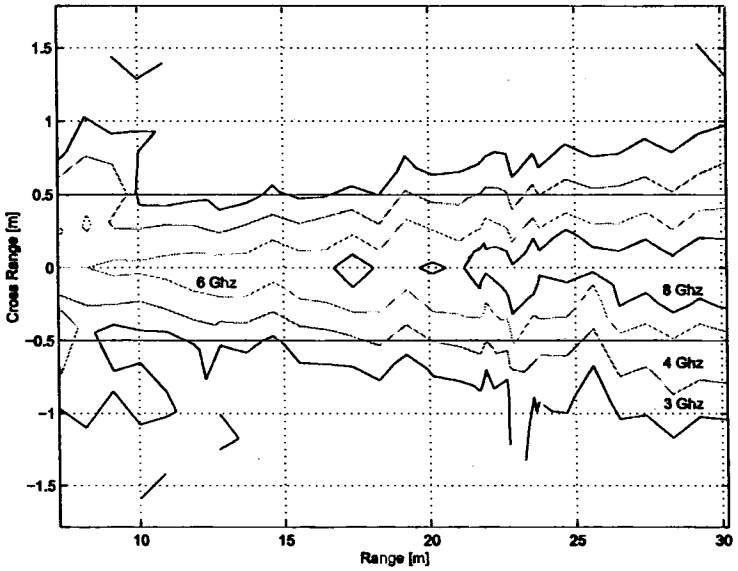

Figure 19: Contours of constant upper 3dB frequency. Further and further from the antenna, there is relatively more high-frequency content. In the far field, these contours should simply expand radially.

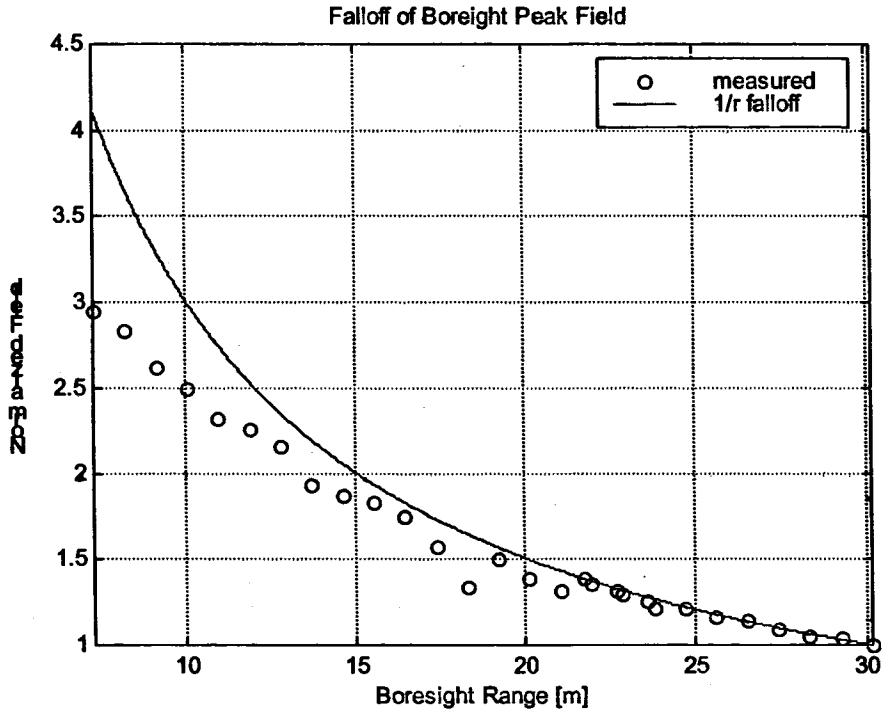

Figure 20: Comparison of the peak boresight field to a curve that falls off as $1/r$. At ranges greater than about 22m, the field fits the curve rather well.

falls off slower than $1/r$ as expected. The near field would be reached when the peak radiated field is approximately constant and only the pulse width changes.

The second of these definitions is considered in fig. 21. Fig. 21 is similar to fig. 18, except in fig. 21, the peak field is multiplied by the range. In the far-field of the antenna, the contour lines should be approximately radial, indicating that the amplitude is falling off as $1/r$ and that the radiation pattern is only a function of angle. In order to ease the examinition, radial lines are plotted corresponding to angle of –5° to 5° in 1° increments (lines at ±½° are also included). For ranges less than 20 m, the radiation pattern is clearly *not* a function of angle alone, and at ranges longer than about 25 m, the contour boundaries seem to be better approximated by radial lines.

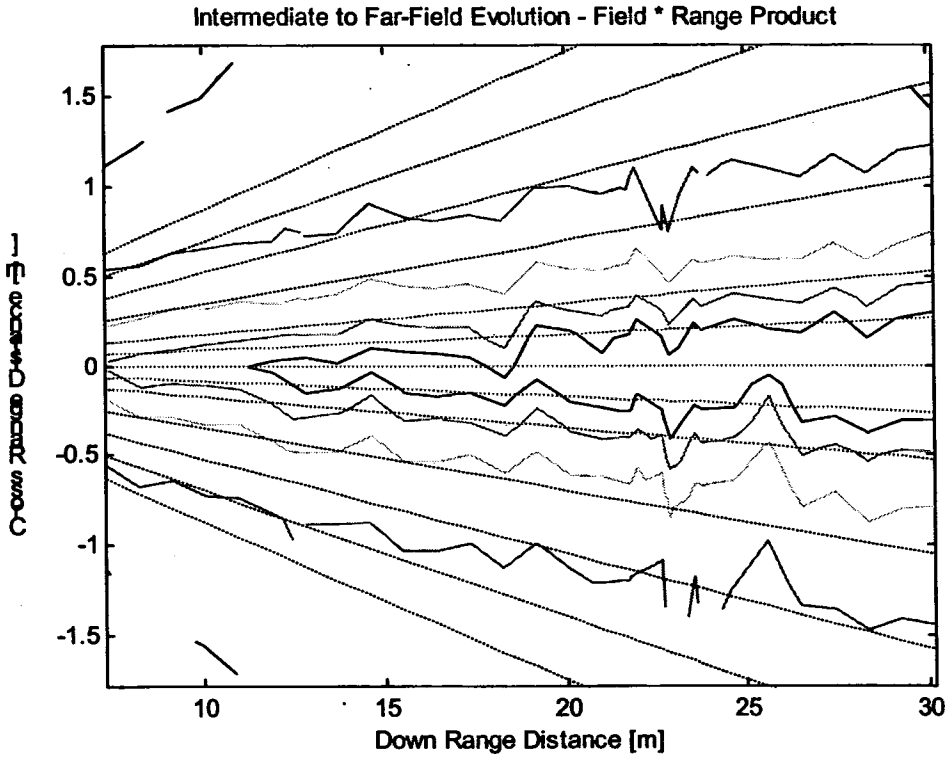

Figure 21: Field-Range product in the main beam of the antenna. At ranges greater than about 25 m, the field-range product is approximately constant in r.

The third definition is considered in fig. 22 where the FWHM pulsewidth of the boresight radiated field is presented as a function of range. As can be seen from the figure, the collected data is not monotonically decreasing, as would be expected, however, at ranges greater than about 25 m, the pulsewidth seems to have settled down to about 35 ps. For a Gaussian pulse, a pulsewidth of 35 ps corresponds to an error function risetime of 38.2 ps. This degradation in risetime (from the 27 ps system risetime) is due to the feed of the antenna.

One of the *a priori* methods of characterizing the far-field of an IRA (without taking data) is to compute the difference in the time of flight from the center and edge of the aperture to

the observation point and comparing that time to the risetime of the applied voltage. Giri, *et al.* [6], suggest that a distance such that the temporal dispersion is 20% of the risetime of the source is safely within the far-field. Farr and Frost [18] propose that when the dispersion is 33% of the risetime, the far field is reached. In fig. 23, the temporal dispersion across the aperture is plotted as a function of downrange distance. The dispersion is calculated from

$$t_d = \frac{\sqrt{(D/2)^2 + r^2} - r}{c}, \tag{3}$$

where D is the diameter of the reflector, r is the range, and c is the speed of light. The solid line in fig. 23 represents the approximate system risetime of 38.2 ps. At a range of 22 m (where the boresight field starts to fall as $1/r$) the temporal dispersion is 19.0 ps (49.5% of the risetime). At a range of 25 m (where the risetime is approximately constant) the temporal dispersion is 16.7 ps (43.6% of the risetime). These results seem to suggest that the estimates made by Giri, *et al.* [6], and Farr and Frost [18] are conservative, and the far-field is closer to the antenna than previously thought. In order to achieve a 20% relation, a range of 54.5 m would have been needed. In order to achieve a 33% relation, a range of 32.7 m would have been needed. This result could be of importance when planning antenna tests where range is limited by outside factors.

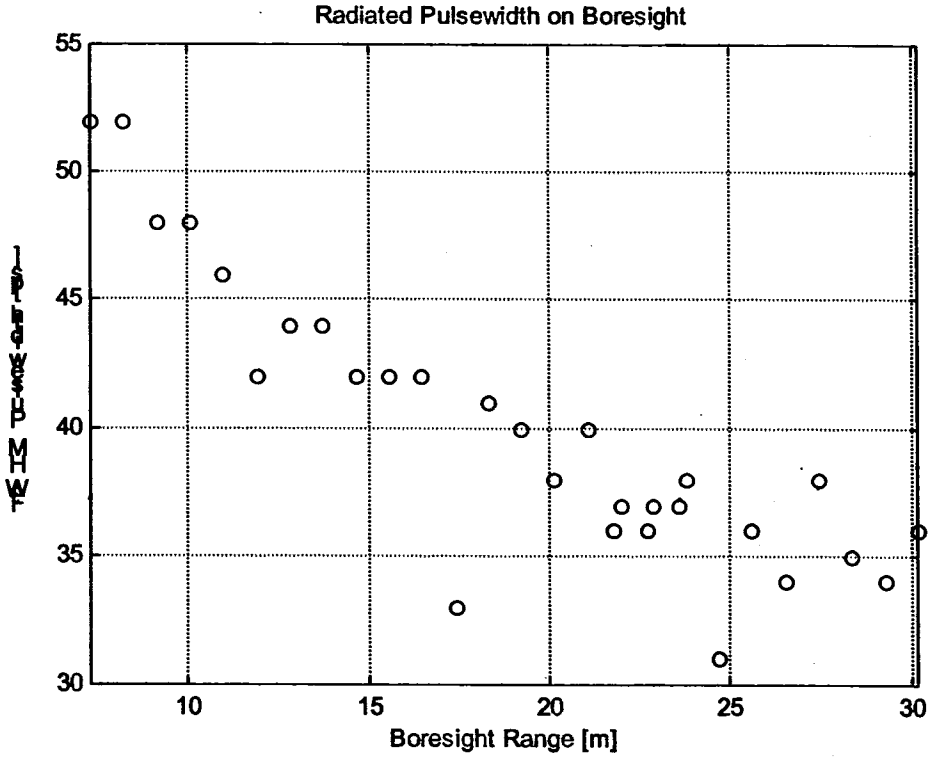

Figure 22: Pulsewidth of the boresight field as a function of range. While the data is not monotonic, at ranges greater than 25 m, the pulsewidth seems to have stabilized to about 35 ps.

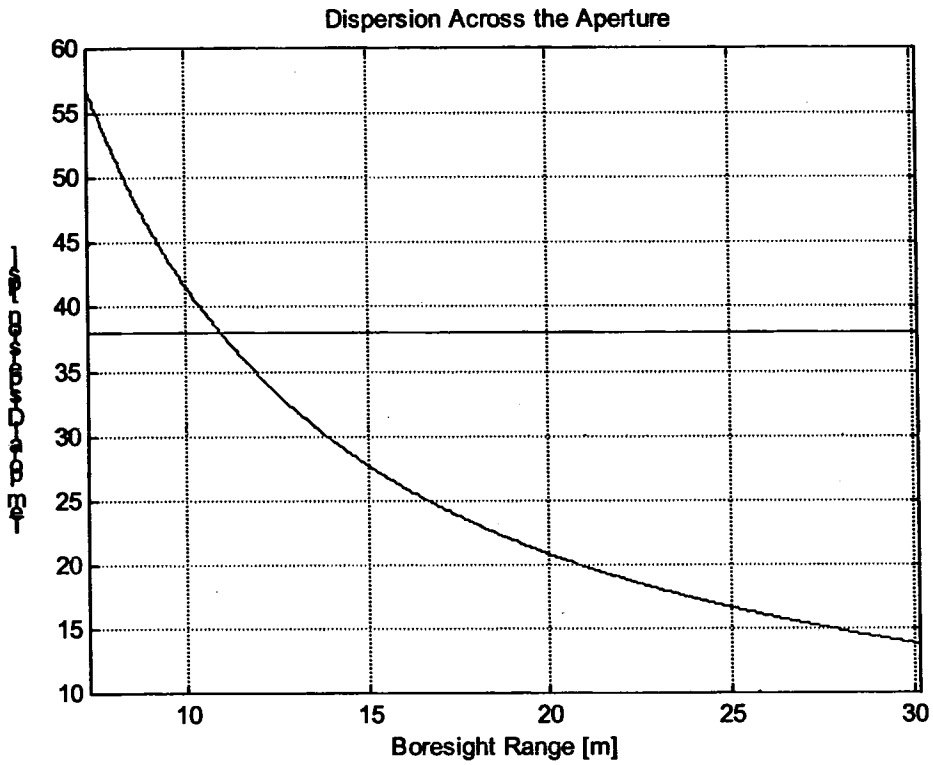

Figure 23: Temporal dispersion computed using (3). The solid line represents the system risetime of 38.2 ps.

5. Conclusions

This study is one of the most thorough investigations of the spatial variation of radiation from an ultra-wideband antenna. While the results are for one particular class of IRA – the HIRA – the general features of the data are applicable to a variety of other types of UWB antennas such as full reflector IRAs, lens IRAs, and TEM horns. While this data set is large by comparison with what is currently available, future measurements should still be made in order to be able to accurately predict the locations of the far-field. In addition, measurements similar to those presented here should be made to explore the near-field/intermediate-field transition zone.

Acknowledgements

The authors would like to thank the following individuals for assistance provided during the experiments and the writing of the report. Leland Bowen and Everett Farr of Farr Research provided use of equipment and discussions concerning the experimental setup and data reduction. Lt. Dave Tifford and Capt. Bret Kreh of AFRL/DEHP aided in data collection. Carl Baum of AFRL/DEHP, Don McLemore of ITT Systems and Science Corporation, and Dave Giri of Pro Tech gave assistance on data interpretation and presentation.

REFERENCES

1. C. E. Baum, "Variations on the Impulse Radiating Antenna Theme" *Sensor and Simulation Notes* #378, February 1995

2. W. D. Prather, C. E. Baum, F. J. Agee, J. P. O'Laughlin, D. W. Scholfield, J. W. Burger, J. Hull, J. S. H. Schoenberg, and R. Copeland, "Ultrawide Band Sources and Antennas: Present Technology, Future Challenges" *Ultra-Wideband, Short-Pulse Electromagnetics 3*, C. E. Baum, L. Carin, and A. P. Stone, Eds., pp. 43-56 (Plenum Press, NY, 1997)

3. E. G. Farr, C. E. Baum, and C. J. Buchenauer, "Impulse Radiating Antenna, Part II" *Ultra-Wideband, Short-Pulse Electromagnetics 2*, pp. 159-170, Plenum Press, New York, 1995

4. L. H. Bowen and E. G. Farr, "E Field Measurements for a 1-meter Diameter Half IRA" *Sensor and Simulation Notes* #419, April 1998

5. E. G. Farr and C. E. Baum, "The Radiation Pattern of Reflector Impulse Radiating Antennas: Early-Time Response" *Sensor and Simulation Notes* #358, June 1993

6. D. V. Giri, H. Lackner, I. D. Smith, D. W. Morton, C. E. Baum, J. R. Marek, D. Scholfield, and W. D. Prather, "A Reflector Antenna for Radiating Impulse-Like Waveforms" *Sensor and Simulation Notes* #382, July 1995

7. E. G. Farr and C. E. Baum, "Prepulse Associated with the Feed of an Impulse Radiating Antenna" *Sensor and Simulation Notes* #337, March 1992

8. C. E. Baum, Personal Communication

9. C. E. Baum, "A symmetry result for an Antenna on a Truncated Ground Plane" *Sensor and Simulation Notes* #415, November 1997

10. O. V. Mikheev, S. A. Podosenov, K. Y. Sakharov, A. A. Sokolov, Y. G. Svekis, and V. A. Turkin, "New Method for Calculating Pulse Radiation from an Antenna With a Reflector" *IEEE Trans. EMC*, **39** pp. 48-54, February 1997

11. C. J. Buchenauer, J. S. Tyo, and J. S. H. Schoenberg, "Antennas and Electric Field Sensors for Ultra-Wideband Transient Time-Domain Measurements: Applications and Methods" *Ultra-Wideband, Short-Pulse Electromagnetics 3*, pp. 405-422, Plenum Press, New York, 1997

12. D. R. Smith, C. E. Baum, R. J. Torres, K. S. H. Lee, and F. C. Yang, "Suppression of Radiation in Unwanted Directions for a Conical Horn (The Microwave Shade)" *Sensor and Simulation Notes* #404, December 1996

13. C. E. Baum, "Intermediate Field of an Impulse-Radiating Antenna" *Sensor and Simulation Notes* #418, December 1997

14. E. G. Farr and C. E. Baum, "Extending the Definitions of Antenna Gain and Radiation Pattern Into the Time Domain" *Sensor and Simulation Notes* #350, November 1992

15. C. E. Baum, "Focused Aperture Antennas" *Sensor and Simulation Notes* #306, May 1987

16. C. E. Baum, "Radiation of Impulse-Like Transient Fields" *Sensor and Simulation Notes* #321, November 1989

17. C. E. Baum, "Aperture Efficiencies for IRAs" *Sensor and Simulation Notes* #328, June 1991

18. E. G. Farr and C. A. Frost, "Compact Ultra-Short Pulse Fuzing Antenna Design and Measurements" *Sensor and Simulation Notes* #380, June 1995